

Flat Spots within Cenozoic Sediments of the Nansen Basin, Arctic Ocean: Indicators for Serpentinization, Gas Generation and Accumulation Processes

S. Yu. Sokolov^{a, *}, W. H. Geissler^b, A. S. Abramova^a, D. A. Ryzhova^c, and I. S. Patina^a

^a *Geological Institute, Russian Academy of Sciences, Moscow, 119017 Russia*

^b *Alfred Wegener Institute Helmholtz Centre for Polar and Marine Research, Bremerhaven, 27568 Germany*

^c *Department of Geology, Moscow State University, Moscow, 119991 Russia*

**e-mail: sysokolov@yandex.ru*

Received April 29, 2022; revised May 31, 2022; accepted June 7, 2022

Abstract—Flat spot anomalies in the Quaternary part of the section of the Nansen Basin are imaged in seismic records and are interpreted to be related to gas-rich fluid accumulations. The flat spots are mainly located above basement highs between magnetic spreading anomalies C20 (~43 Ma) and C12 (~33 Ma). The complex morphometric analysis of flat spots show that serpentinization processes identified from modelling of gravity anomalies could be original gas source. This process also makes smoothing of the basement highs amplitudes. The depth of the top of the flat spots below the seafloor has an almost constant value of ~390 m indicating the ascent of gases from variable basement depths to a common subsurface fluid trap. The depth of the anomalies below the seafloor corresponds to a theoretical thickness of gas hydrate stability zone in the studied region. Gravity modeling along the Arktika-2011-03 section showed the position of the upper mantle blocks with lower (to 2.95 g/cm³) density within the highs of the acoustic basement. The flat spot anomalies occur above basement highs, below which blocks with lower density typical of serpentinized rocks are modelled. Thus, the serpentinization of the upper mantle ultramafic rocks is considered a main geochemical process, which can explain generation and accumulation of gas in oceanic abyss at a 1–3 km thick sedimentary cover, as well as small vertical movements of the basement blocks due to density reduction and expansion of serpentinized rock.

Keywords: methane, flat spots, ultra-slow spreading, serpentinization, Nansen Basin, seismic data, gravity modeling

DOI: 10.1134/S0024490222060074

1. INTRODUCTION

Ultraslow spreading is observed on the segments of global mid oceanic ridge (MOR) system, which have particular geological features distinguishing them from the other parts of MOR (Astafurova et al., 2000; Edwards et al., 2001; Okino et al., 2002; Jokat et al., 2003; Michael et al., 2003; Dick et al., 2003; Klein, 2003; Snow, Edmonds, 2007; Curewitz et al., 2010). Main peculiarities of ultraslow ridges are the general poor magma production, missing of a normal oceanic crust elements (pillow lavas, sheeted dykes etc.) and rough oceanic basement morphology. Rifting under amagmatic conditions leads to unroofing of upper mantle peridotites which in low temperature environment and contact with water provide the material for serpentinization processes. Serpentinization causes significant density loss of the affected rocks, diagenetic upward tectonic movements, and methane generation (Charlou et al., 1998; Bougault, 2012). The majority of ultraslow ridge segments is not surrounded

by significant sedimentary cover, which could trap the abiotically generated methane (Petrov et al., 2016). The oceanic basement of the Nansen Basin as the southern part of Eurasian Basin was formed at the ultraslow-spreading Gakkel Ridge. According to magnetic anomalies spreading in Nansen Basin started at 56 Ma (Nikishin et al., 2020). The sedimentary cover of the Nansen Basin has average thickness ~3 km reaching 6 km in the eastern part (*Arctic Basin ...*, 2017), due to the high sediment input from the Eurasian and Laptev Sea shelves. In the eastern part of the basin even the Gakkel Ridge itself is completely covered by sediments from the Laptev Sea shelf sedimentary fan (Baranov et al., 2019). The thick sedimentary cover in the Nansen Basin provides the conditions for trapping of fluids as can be observed by flat spots on the seismic sections, a typical hydrocarbon indicator (Taner et al., 1979) for sedimentary basins with mature conditions for hydrocarbon generation. Flat spots in the central parts of the Nansen Basin show the pres-

ence of free gas in the upper parts of sedimentary section with total thickness less than 2 km (*Arctic Basin ...*, 2017) above oceanic basement, which accretion occurred in ultraslow spreading conditions. Similar observations of free gas accumulations were made on the flanks of other Arctic ultraslow spreading ridges west of Svalbard covered by sediments (Johnson et al., 2025; Waghorn et al., 2018).

Progress in seismic studies of deep-sea Arctic allowed the development of a substantial and consistent tectono-sedimentary model, which includes main ideas on geology and seismo-stratigraphy (Jokat and Micksch, 2004; Engen et al., 2008; *Arctic Basin ...*, 2017; Nikishin et al., 2020). We identified flat spot anomalies of fluid origin (according to indirect evidences) in the data of Arktika-2011 project (*Arctic Basin ...*, 2017) in the upper part of the section of the Nansen Basin and are distinct from magmatic-related bright spots observed beneath the Barents Sea shelf. Stratigraphically, these anomalies occur in the middle part of Quaternary sediments and exhibit no links to strong lithological reflectors. The fluid most likely derives from methane-producing serpentinization of the upper mantle rocks, which were studied in many deep-sea regions of the World Ocean with total sediment thickness not greater than 3 km. Methane either forms a plume in seawater or accumulates in topmost parts of sedimentary cover yielding a characteristic record in a seismic wave field (Charlou et al., 1998; Bougault, 2012; Baranov et al., 2019; Shakhova et al., 2017).

This study includes mapping and analysis of spatial distribution of seismic flat spots in combination with potential field data, 2D gravity modeling of crust and upper mantle structures with serpentinized blocks and comparison of flat spot morphometric characteristics with geophysical fields. This comparative analysis of several parameters, such as width of the flat-spot, amplitude of the basement high and the thickness of the sedimentary layer above and beneath the seismic anomaly in combination with potential field data can show causal relationships for a better understanding of their genesis and role in tectono-sedimentary processes. Our study aims to better understand the origin and geodynamic setting of the flat spots.

2. REGIONAL SEISMIC STRATIGRAPHY AND FLUID ORIGIN

2.1. Regional Seismic Stratigraphy

Because the ice-covered Arctic basins are difficult to access, the knowledge and understanding about the evolution of the upper mantle, crystalline crust, and the sedimentary cover develop slowly in comparison to ice-free oceanic basins. Nonetheless, available seismic data for and Nansen Basin (Fig. 1) generally characterize its geological structure and stratigraphy (Jokat et al., 1995; Weigelt and Jokat, 2001; Geissler and

Jokat, 2004; Jokat and Micksch, 2004; Engen et al., 2009; More and Pitman, 2011; Hegewald and Jokat, 2013; *Arctic Basin ...*, 2017; Nikishin et al., 2017; Castro et al., 2018; Lutz et al., 2018). The various multichannel seismic reflection and seismic refraction data are a basis for our detailed study of the region (Sokolov et al., 2019).

Joint seismostratigraphic division of the sedimentary cover for the Norwegian and Russian sectors of the Nansen Basin is shown in Fig. 2 after (Engen et al., 2009) and (*Arctic Basin ...*, 2017; Nikishin et al., 2017), respectively. Comparison of horizon ages in Fig. 2 is made having no direct tie to chronostratigraphic framework proved by drilling between the data in Norwegian and Russian sector of Nansen basin. Engen et al. (2009) studied the western part of the Nansen Basin and its frame using the data of (Jackson et al., 1984; Baturin et al., 1994; Riis, 1994; Jokat et al., 1995; Sorokin et al., 1998; Weigelt and Jokat 2001; Jokat et al., 2003; Geissler and Jokat, 2004; Jokat and Micksch, 2004). According to this work, four seismic units with typical seismic interval velocities from 1.8 to 2.4 km/s have been recognized in the sedimentary cover. Recently, Lutz et al. (2018) studied the seismic stratigraphy of the sedimentary cover and a basement configuration of the southwestern part of the Eurasian basin.

A series of reflection horizons are interpreted within vast territories based on seismostratigraphic data (Fig. 2). The acoustic basement, used for Fig. 2 (Engen et al., 2009) is traced from the continental shelf and is characterized by diffraction hyperbolas from the irregular top of the oceanic basement in the unmigrated seismic data. There is onlap on existing basement topography of a thick unit of undeformed sedimentary rocks. The age boundaries of NB-1A, NB-1B and NB-2 units differ according to different authors (Jokat and Micksch, 2004; Engen et al., 2009; Nikishin et al., 2017) (Fig. 2). Nikishin et al. (2017) identified four seismic units generally typical of the Eurasian Basin: (i) Early to Mid Eocene (56–45.7 Ma), (ii) Mid Eocene to Early Oligocene (45.7–33.2 Ma), (iii) Early Oligocene to Early Miocene (33.2–19.7 Ma), and (iv) Early Miocene to Present (19.7–0 Ma). Engen et al. (2009) subdivided the section into subunits, especially, the Upper Miocene–Quaternary period. Below, we describe the youngest seismic unit NB-4 according to (Engen et al., 2009).

Seismic unit NB-4 consists of the Quaternary (2.6–0 Ma) sediments. The conformal boundary between units NB-3 and NB-4 is concordant and is traced as a continuous reflection horizon of medium amplitude. Interval velocities of the seismic unit vary from 1.6 to 2.0 km/s (1.8 km/s, on average) and its thickness is 0.4–0.6 km (Engen et al., 2009). The bottom of the unit in one profile exhibits a ~0.1 km thick debris flow deposits with loss of reflection coherence typical of chaotic clastic sediments. The presence of

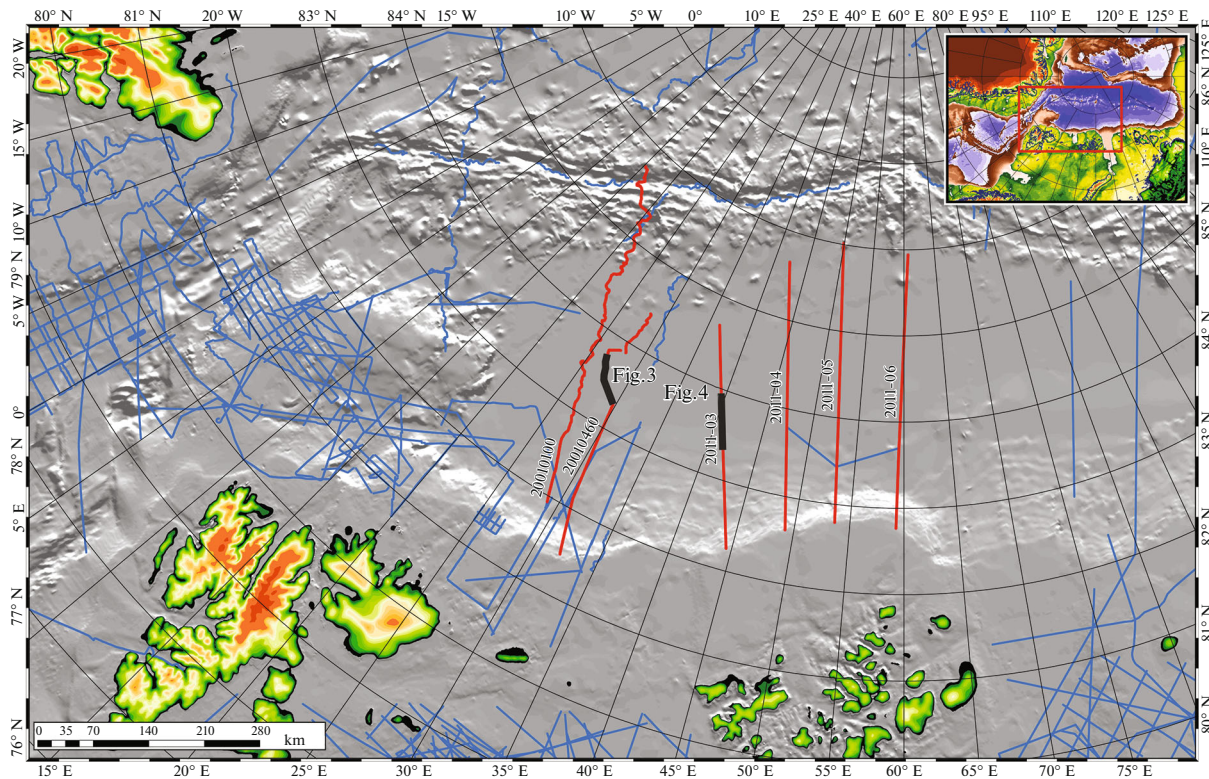


Fig. 1. Seismic data for western Arctic and Nansen Basin in 2014 according to Alfred Wegener Institute for Polar and Marine research (Bremerhaven) and VNIIOkeangeologiya (St. Petersburg). Red, section used in this study; solid black lines, fragments of sections shown in Figs. 3 and 4.

similar sedimentary bodies in other basin parts is expected. According to the seismic record, NB-4 unit is subdivided by (Engen et al., 2009) into two subunits: the lower (NB-4A) showing weak parallel horizons and local acoustic blanking of the record with loss of reflection coherence and the upper (NB-4B) showing striking parallel reflections, which are much brighter than underlying ones. These are interpreted as two regional subunits formed as a result of erosion of a glacial slope in Pleistocene (Geissler and Jokat, 2004; Engen et al., 2009).

2.2. Origin of Fluid

Several studies of oceanic rifts with exposed mantle ultramafic rocks without sedimentary cover have identified the high (by several orders of magnitude) contents of CH_4 dissolved in bottom waters, proven the abiogenic origin of hydrocarbon (CH_4) on the basis of $\delta^{13}\text{C}$ isotopic composition (Charlou et al., 1998; Dmitriev et al., 1999; Keir et al., 2005; Bougault, 2012). Seawater circulation through the upper mantle ultramafic rocks along deep-reaching fault system results in serpentinization at temperatures of 100–450°C, the formation of serpentine and magnetite after olivine, and the release of H_2 , which interacts with seawater-dissolved CO_2 , thus producing CH_4

(Charlou et al., 1998; Dmitriev et al., 1999). Discharging of fluid serpentinization products into the poorly consolidated water saturated sediments creates accumulations and form a seismic record typical for gas-rich conditions.

Oceanic crust formed at slow- and ultraslow-spreading with minor basaltic and gabbroic layers and the presence of sedimentary cover able to trap the fluid are most favorable for this process. In sediment-free conditions, CH_4 directly goes to the water column. For example, that was detected along the eastern flank of the Knipovich Ridge (Cherkashev et al., 2001). Assumption on its origin from serpentinized rocks was made by (Rajan et al., 2012).

In addition to origination of fluids (Dmitriev et al., 1999), serpentinization is accompanied by the formation of a new magnetic layer due to crystallization of magnetite and change of the primary magnetic anomalies pattern (Astafurova et al., 1996; Oufi et al., 2002), the volumetric extension of serpentinized rock and decreasing of its density to 20% (*Physical ...*, 1984), and the enhanced heat flow due to exothermic effect (Delescluse and Chamot-Rooke, 2008). The scarce measurements of heat flow in the deep-sea polar area (Khutorskoy et al., 2013) do not allow correct estimation of serpentinization heating contribution to its value. Density reduction, which accompanies ser-

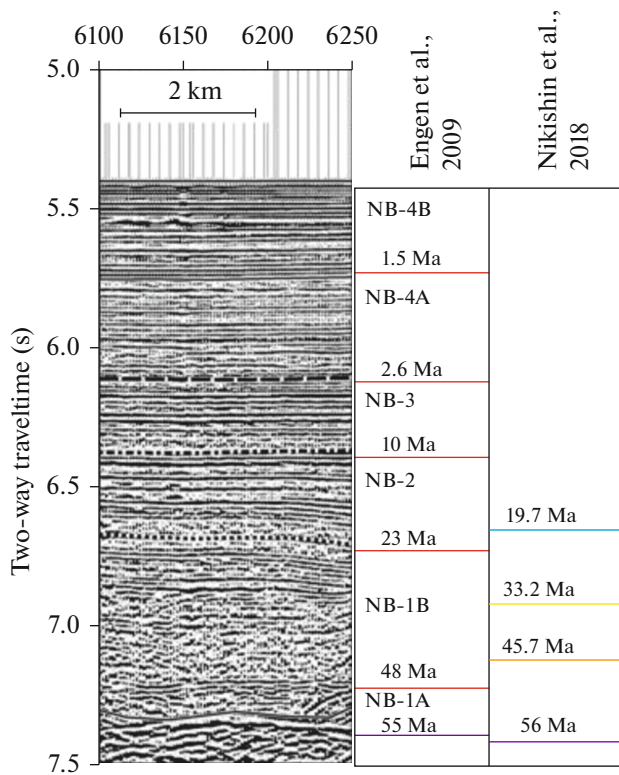


Fig. 2. Main seismic units in the Norwegian (modified after (Engen et al., 2009)) and Russian (modified after (Nikishin et al., 2017)) sectors of the Nansen Basin.

pentinization and expands the rock volume (*Physical ...*, 1984), explains the positive vertical movements of crystalline crust blocks and the formation of a fault network in sedimentary cover and fluid pathways.

3. FLAT SPOT DATA AND THEIR ALLOCATION

3.1. Flat Spot Pattern on Seismic Section

Flat spot anomalies were observed in the Nansen Basin in seismic sections of AWI expeditions (Fig. 3) and the Arktika-2011 project (Fig. 4). In all cases, they represent a higher amplitude reflector of a few kilometers in width in the section plane above large highs of the acoustic basement. According to the displacement of the positive and negative reflector phases, evidences for reverse faults and local highs in reflector configuration of the section upper part (indicating vertical displacements of the basement blocks) are observed above these basement highs. In some cases, the faults are developed throughout the entire sedimentary cover indicating a present-day tectonic process. There are also indications of narrow vertical zones of acoustic blanking and changes in the amplitudes of the reflectors near such zones. This is evidence of possible ascent of fluids and horizontal fluid flow.

In case of fluid or gas saturated rock the seismic signal should be marked by inversion of polarity due to negative contrast of acoustic impedance relative to ambient rocks (Taner et al., 1979). Seemingly similar anomalies of seismic record could occur, for example, in sections with sills in sedimentary sequence, located in the northern part of the Barents Sea shelf (Startseva et al., 2017). But these anomalies are unparallel to sedimentary beds, have positive polarity and high amplitude of reflections, and should be referred to bright spots rather than flat spots. Another distinction is related to uneven reflections from igneous intrusions, which have variable inclination angles and often intersect phases reflected from sedimentary cover. Such anomalies were drilled at Ludlow area of Barents Sea (Burguto et al., 2016) and were found to be Jurassic–Early Cretaceous mafic intrusions (*Map of Prequaternary formations*, 2004).

The polarity of the Nansen Basin flat spots (Fig. 4) is distinct from the seafloor reflection due to a negative jump of impedance, which is a result of fluid accumulation in porous rock (Taner et al., 1979). Thus, in case of lack of direct drill core sampling, this signal property is indirect but certain evidence of fluid origin of the anomaly. All flat spots in the Nansen basin are smooth and horizontal indicating fluid origin of anomalies, the lower boundary of which get this kind of shape after fluid upward migration and accumulation beneath the trap.

3.2. Flat Spot Allocation in Sedimentary Section

Another feature of flat spots in Nansen basin is related to their stratigraphic location, as a rule, in the middle part of the NB-4 unit rather than associated to reflector, which limits this (or another) seismic unit (Fig. 4). Flat spot are related to horizontal fluid accumulations below the sedimentary layers with impermeability (Backus and Chen, 1975), which could originate not only from varying lithology, but from physical state of fluid saturated rocks such as gas hydrate (Judd and Hovland, 2007), which disruption could lead to seepage of gas through the sea bottom into water column. In Fig. 4, the anomaly occurs in the middle of seismic unit NB-4A, the lower part of which contains debris flow sediments responsible for transparent incoherent signal (Engen et al., 2009). These sediments most probably originated after sea level fall and enhanced contribution of eroded sedimentary material from the shelves and islands to the basin in the beginning of Pleistocene (Engen et al., 2009). Flat spot reflectors in Nansen basin also have higher relative amplitudes in contrast to acoustic properties of fluid-free ambient rock.

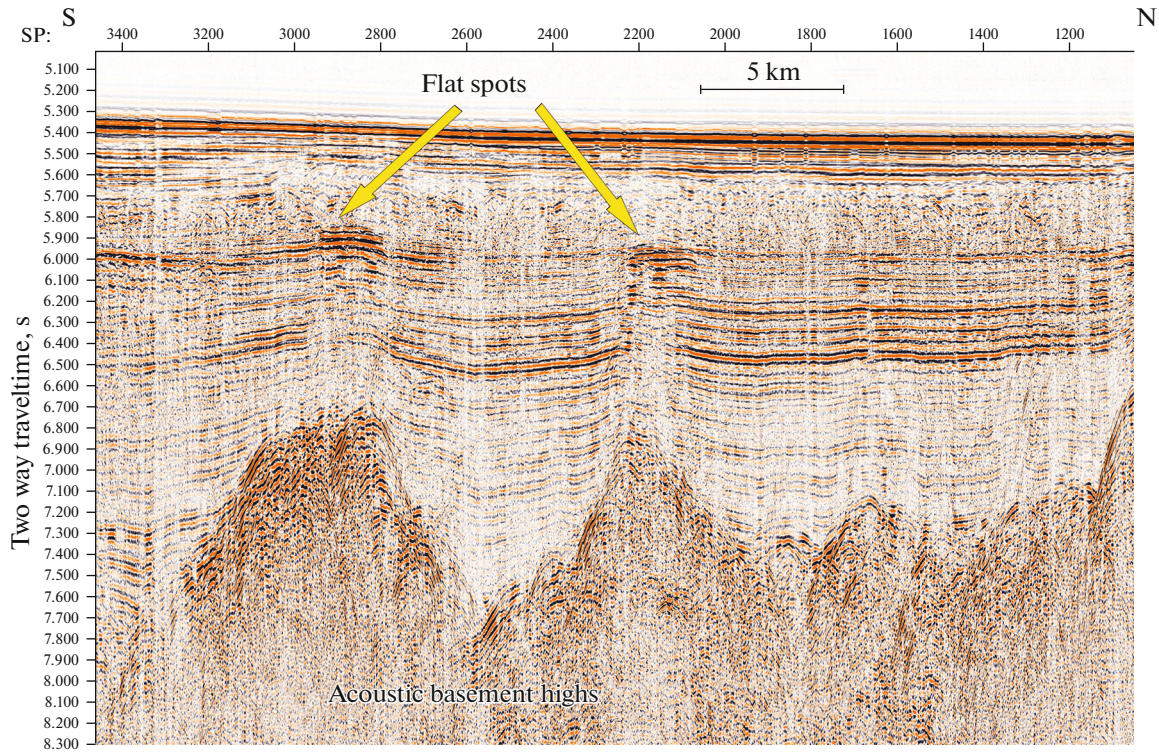


Fig. 3. Fragment of AWI 20010460 section (for position, see Fig. 1) with flat spot anomalies of seismic record above the acoustic basement protrusions.

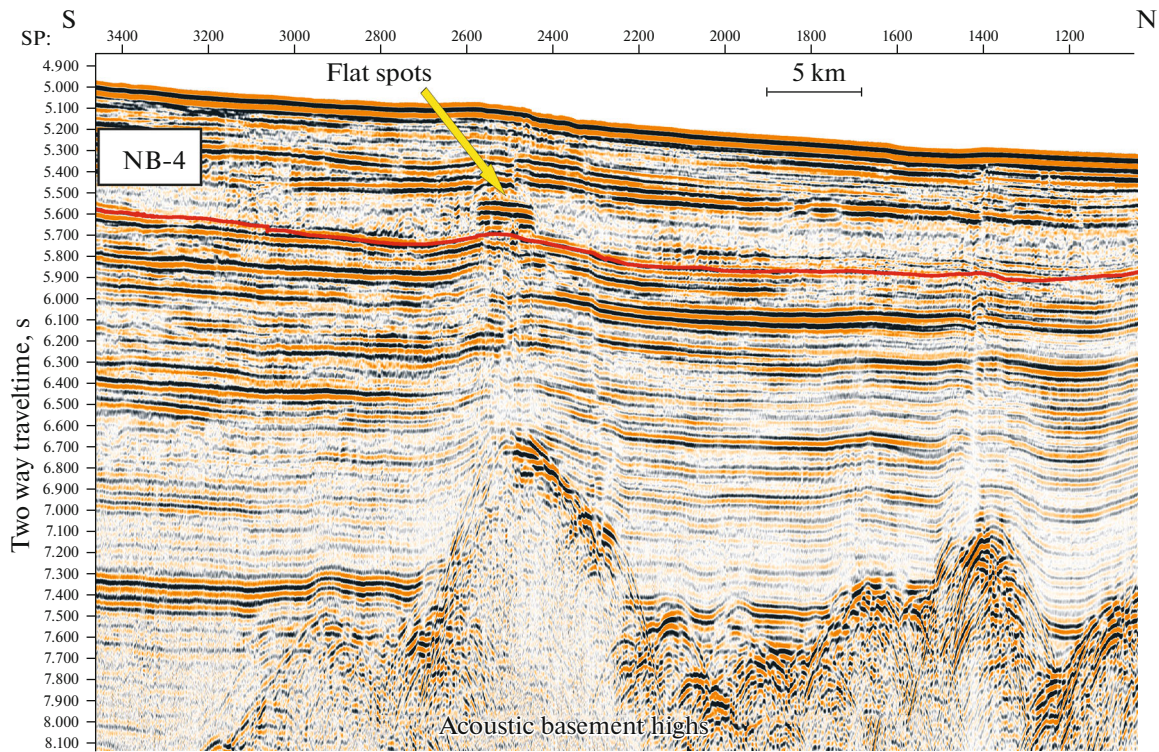


Fig. 4. Fragment of Arktika 2011-3 section (for position, see Fig. 1) with flat spot anomalies of seismic record above the acoustic basement protrusions. Red line, interpretation of the position of the bottom of seismic unit NB-4 (Fig. 2).

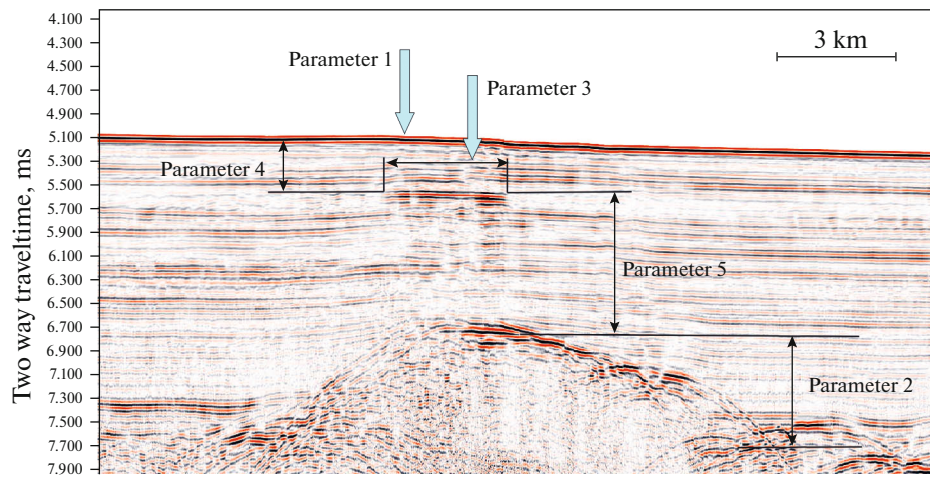


Fig. 5. Fragment of Arktika 2011-3 section with flat spot anomaly of seismic record above the acoustic basement protrusion. Parameters: (1) bottom depth in the area of the anomaly (m); (2) basement protrusion high over the average value of ambient rock (ms); (3) spot width (m); (4) thickness of sediments above the spot (ms); (5) thickness of sediments between the spot and the basement protrusion (ms).

4. METHODS OF DATA ANALYSIS

4.1. Mapping of Flat Spot Anomalies

Time domain stack seismic sections AWI-20010100 and AWI-20010460 with a CMP distance of 25 m and Arktika-03, -04, -05, and -06 with a CMP distance of 6.25 m were interpreted in the RadExPro-2018.4 software using picking of the tops of the flat spot anomalies as an individual horizon beyond the current seismic stratigraphic scheme (Fig. 2). The study deals with the objects allocated within upper 500 ms below bottom and not needed in depth migrated seismic data for area with water depth ~4000 m. Positions of flat spot tops obtained from seismic section interpretation becomes a spatial objects on different topographic basemaps.

4.2. Morphometric Characteristics of Flat Spots

We digitized flat spots morphometric characteristics, the geometry of which is shown in Fig. 5. The following parameters of the anomalies were chosen: (1) the seafloor depth, (2) the vertical amplitude of the basement high, (3) the width of the anomaly in section plane, and the thickness of the sedimentary layer (4) above and (5) beneath the anomaly. We also used the total intensity of magnetic anomalies ΔT_a (Maus et al., 2009) and Bouguer gravity anomalies (Balmino et al., 2012) to compare with listed above parameters for their geodynamic and structural interpretation. This approach was examined on material of deep-sea areas of an equatorial segment of the Atlantic Ocean before (Sokolov, 2017), which exhibits deformations of the basement and sedimentary cover with significant acoustic blanking of seismic sections related to free gas discharge. The comparison of morphometric parameters of deformations with values of geophysical fields

allowed conclusions on impact of crustal and upper mantle on the structure and deformations of sedimentary cover. Similar approach is applied here for the Nansen Basin flat spot anomalies and it can be a key for understanding of their genesis and place in a causal sequence of tectono-sedimentary processes.

4.3. 2D Gravity Modeling

Serpentinization, which is accompanied by density reduction of the upper mantle rocks, provides the basis for local changes in standard density model of the crust and uppermost mantle and for verification of the hypothesis of these changes by solution of the forward modeling. The free air gravity anomalies along the Arktika-2011-03 section were simulated in TG-2D program by forward and inverse gravimetry solutions using interactive selection of gravity effects depending on 2D structural-density blocks (Bulychev and Zaitsev, 2008). The section is approximated by a system of closed rectangles with a constant density (g/cm^3). The formation of 2D model requires the depth of the boundaries of main layers and their densities. The interpretation of Arktika-2011-03 section yielded the depth values of seafloor and acoustic basement, which were recalculated from time domain with seismic velocities of 1500 and 2000 m/s for the water column and sedimentary layer, respectively. The free air gravity anomalies along seismic section line were obtained from the WGM-2012 model (Balmino et al., 2012).

The model includes four main layers, the gravity effect from which has different amplitude characteristics. The bottom of the first (water) layer with a density of 1.03 g/cm^3 is determined by seafloor bathymetry from IBCAO version 3 (Jakobsson et al., 2012). The bottom of the second (sedimentary) layer is identified

from seismic data, which shows units from modern to Early Eocene (Nikishin et al., 2017). For this layer we assume average density of 2.30 g/cm^3 , as typical for mainly clay rocks (*Physical ...*, 1984). This assumption is supported by core physical properties from ODP site 911 (Myhre et al., 1995), which has linear trend of density from 1.8 to 2.1 g/cm^3 in the upper 400 m of core. Average density through entire sedimentary cover with thickness up to 4.5 km in southern part of section (*Arctic Basin ...*, 2017) should be set to bigger value. Assessment of velocity for Cenozoic sedimentary rock by L.Y. Faust formula (Faust, 1951) and velocity-density relationships by G.H.F. Gardner (Gardner et al., 1974) allows the value of 2.3 g/cm^3 .

The available seismic reflection data did not image the reflection the Mohorovicic discontinuity (Moho), which is the boundary between the crust and the upper mantle. Due to lack of seismic refraction data, a common practice is to accept a suggestion on a crystalline crust layer with a constant thickness of 6000 m (Kuo and Forsyth, 1988), which was used for the Mid-Atlantic Ridge zone with spreading half rates of 2–4 cm/year. In segments of slow- and ultraslow-spreading ridges (half rates of $<15 \text{ mm/year}$) with reduced magmatism, this value should be decreased. A review of data on the refracted waves and crustal models in the basins adjacent to such ridges (Ritzmann et al., 2002, 2004; Ljones et al., 2004; Czuba, 2007; Kandilarov et al., 2008, 2010; Hermann and Jokat, 2013; Schmidt-Aursch and Jokat, 2016) shows plausible suggestion on a crystalline crust layer 4000 m thick from the top of the acoustic basement. The density of 2.85 g/cm^3 is modelled for the third layer with a bottom at the Moho boundary. The upper mantle rocks with a density of 3.30 g/cm^3 are modelled below the oceanic crust. Refusal of constant crust layer thickness for approaching of model fit without measurements of Moho depth from reflection or refraction data could lead to wrong model configuration in the places where observed field is contributed by density variation.

Fit of computed field to measured field by forward modelling does not have a single solution. It could be derived by numerous versions of density distribution. From our point of view preferred version is that maintains the blocks with biggest difference in density within the layers first of all. For serpentinized mantle it shifts from 3.3 to 2.95 g/cm^3 . Therefore, lesser variations of density in other layers could be not in main consideration. In other words, we do not have information about allocation of small density variations in crust, but we have manifestations of variations in upper mantle. The fitting approach should be done in this layer fixing other layers with constant density. Search of fit will be done by changing of size of supposed serpentinized blocks. Varying of smaller density difference in the crust is a less justified approach for the task in Nansen basin.

5. RESULTS OF DATA ANALYSIS AND ITS PRIMARY INTERPRETATION

5.1. Spatial Distribution of Flat Spot Anomalies

The positions of mapped anomalies along seismic sections are shown in Fig. 6, as well as the thickness of the sedimentary cover as a topographic base (Petrov et al., 2016). Within the limits of studied sections, we identified 22 flat-spots that are more or less concentrated in a band between magnetic anomalies C20 ($\sim 43 \text{ Ma}$) and C12 ($\sim 33 \text{ Ma}$) (Fig. 6). This age range of the basement (spanning the Middle and Late Eocene), prompts the search of tectonic regime changes as a reason for the regional basement structure formation in this time. In areas near to continental slope with a $>3 \text{ km}$ thick sedimentary cover no flat spots were discovered in seismic data of Arktika-2011 project.

5.2. Morphometric Characteristics of Flat Spots

The studied sections exhibit 22 flat-spot anomalies in total, which is insufficient for reliable statistical estimations of morphometric properties, however, some conclusions can be drawn. Symbol size scaling by third parameter values yields additional aspects during 2D cross-plotting. Less values of Bouguer gravity anomalies at the places of flat spots indicate the decreasing of basement density with wider seismic record anomalies, shown by symbol scaling (Fig. 7a). It shows greater volume of accumulated gas due to strong serpentinization of ultramafic rocks, which leads to decrease in their density. Lower differential basement topography (difference between basement highs and lows) at smaller Bouguer values (Fig. 7a) can be explained by its reducing with the development of upper mantle reworking and increase of area involved in serpentinization. The comparison of anomalous magnetic field values with a flat spot width (Fig. 7b) shows a weak trend of its growth with increasing of magnetic positive anomalies (probably overprinted on primary linear anomaly structure and having Brunhes age), because gas-producing serpentinization is accompanied by the formation of magnetic minerals (Astafurova et al., 1996). Fig. 7b also shows the transfer of negative anomalies to positive values with the growth of flat spot width. Scaling by the amplitude of the basement differential shows that formation of wide flat spots result in smaller difference between irregularities of underlying basement. It primarily could be interpreted as the result of the serpentinization process evolution.

Considering Fig. 8, the comparison of morphometric parameters reveals reasonable correlations: the less the differential of the basement, the thicker the sediments between the basement and the anomaly and wider the flat spot anomalies shown by symbol scaling on Fig. 8a and by basement differential scaling on Fig. 8b. The key is that the evolving serpentinization leads to

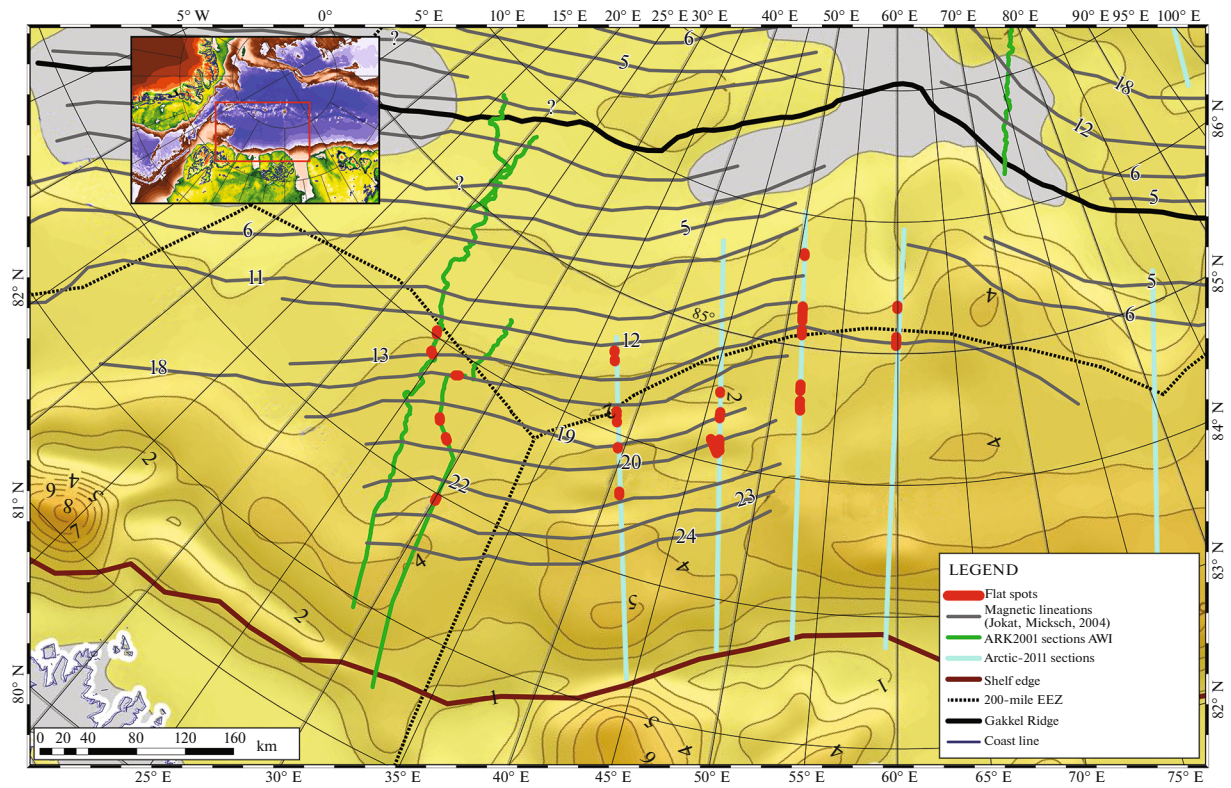


Fig. 6. Spatial distribution of flat spot anomalies in the Nansen Basin and position of linear magnetic anomalies according to (Jokat, Micksch, 2014). The thickness of sedimentary cover (km) is used as a topographic basis, after (Petrov et al., 2016).

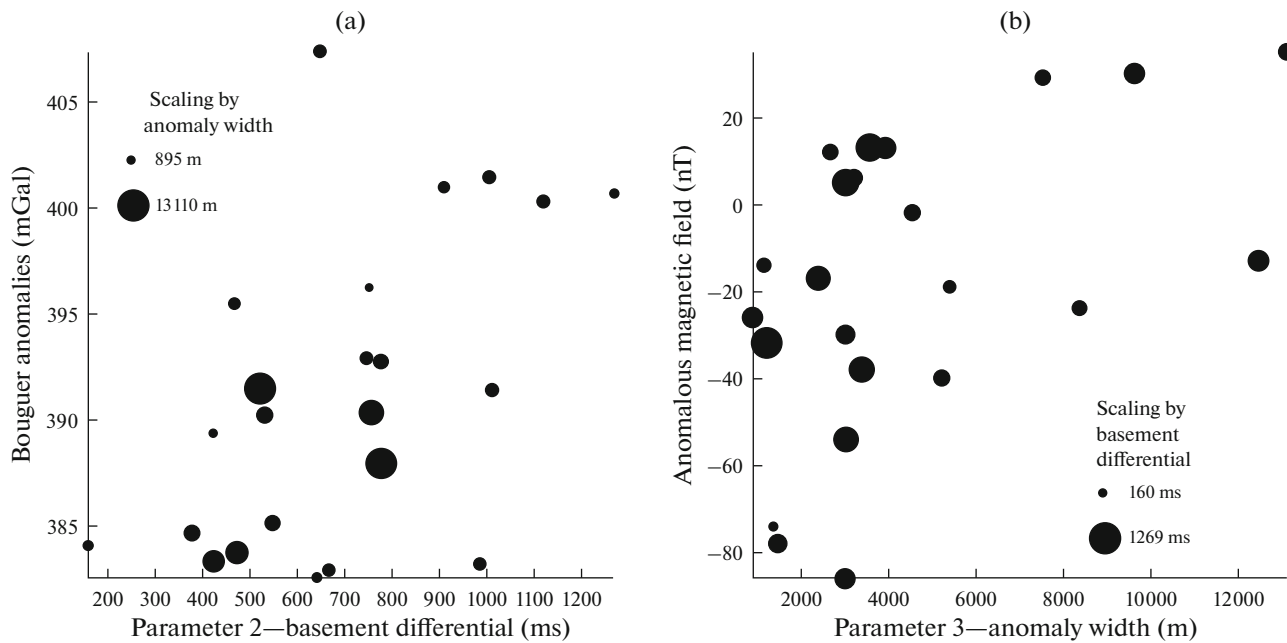


Fig. 7. Cross-correlation of geophysical fields and morphometric parameters of flat spot anomalies: (a) Bouguer anomalies after (Balmino et al., 2012) and difference in the basement protrusions; (b) anomalous magnetic field ΔT_a after (Maus et al., 2009) and the width of flat spots. Herein and in Fig. 8, linear scaling of symbols is by parameters 3 ((a) spot width) and 2 ((b) amplitude of basement protrusion). The minimum and maximum sizes of symbol scaling are conditional.

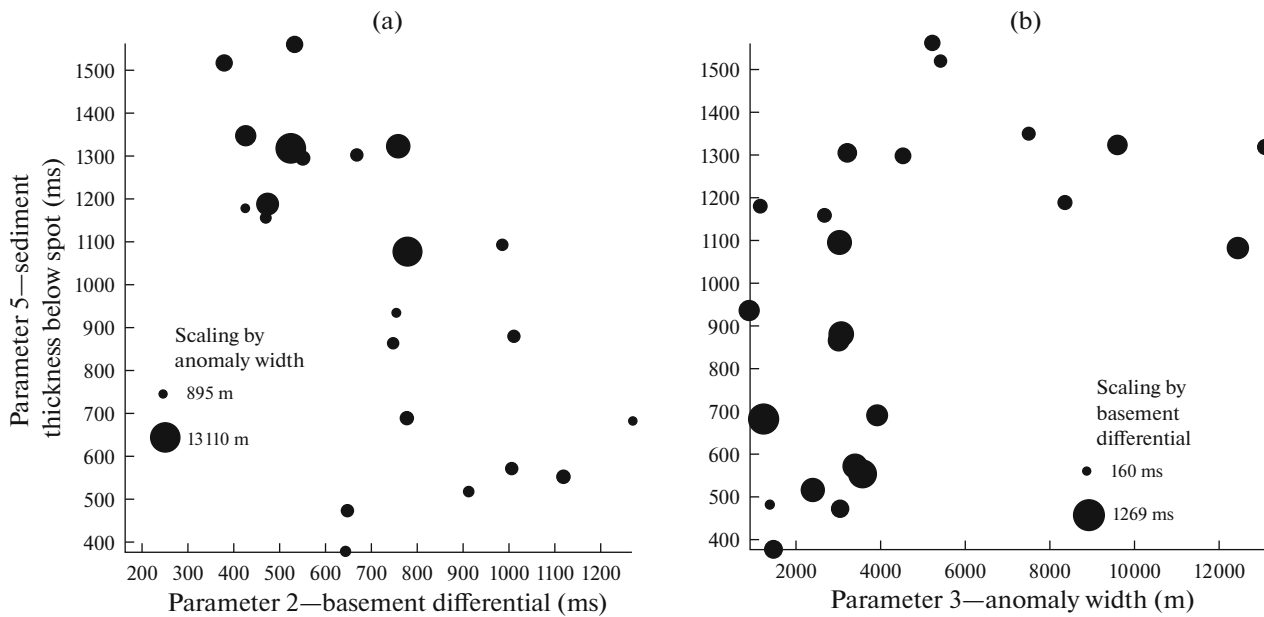


Fig. 8. Cross-correlation of morphometric parameters of flat spot anomalies: (a) difference in basement protrusions with thickness of sedimentary cover below the spot; (b) width of flat spots with thickness of sedimentary cover below the spot.

greater gas discharge and smoothed basement highs, probably, due to expansion of the area around primary irregularity of serpentinization center. It also should be noted, that all flat spot anomalies are mostly located above a narrow range of Bouguer anomaly values of 380–390 mGal (Fig. 9).

Parameter 4 (two way traveltime depth of the anomaly below the seafloor or sedimentary thickness above anomaly) is almost spatially constant along 22 detected anomalies and is 490 ± 100 ms with significant variation of sediments thickness below flat spots (from 378 to 1562 ms). Assuming a seismic P wave velocity in the upper part of the section of 1600 m/s, the average values of parameter 4 will be 390 m. The constant depth of the anomalies could be explained by the vertical migration of free gas towards the base of the gas hydrate stability zone where it form trap and accumulates in it. Following to (Wallman et al., 2012), the predicted thickness of the stability zone of a gas hydrate layer in the area of study is 370–400 m: this is similar to the observed depth of the anomalies.

Scaling of anomalies position by flat spot width (Fig. 9) shows that this parameter increases towards the East within the Nansen Basin. It could be the evidence of more intense accumulation of gas in the eastern anomalies and also of more gas beneath the spots in the sedimentary column. Based on available data, it is difficult to conclude that this is a result of increasing area of serpentinized ultramafic rocks.

5.3. 2D Gravity Modeling Along the Arktika-2011-03 Line

The modeling results are shown in Fig. 10. The model calculations of four layers with a constant density of 3.30 g/cm^3 for the upper mantle, excluding the serpentinized blocks with a density of 2.95 g/cm^3 (Fig. 10a), yield higher (by 8–12 mGal) calculated field relative to the observed field in areas of the acoustic basement highs (Fig. 10a). To compensate the differences, the blocks with a density of 2.95 g/cm^3 , typical for density reduced serpentinized mantle (Physical ..., 1984) were included into the model using interactive selection, thus achieving the ± 1 mGal (or less) difference between the total model effect and observed gravity field, which provided reduced differences. Three boundaries, which were measured from seismic section and proposed for bottom of crystalline crust with constant 4000 m thickness, remain unchanged: seafloor, acoustic basement, and the Moho. Topography of the Moho could have an effect on the modelling but there are no data on it. Therefore, a constant thickness for the crust was assumed. The maximum difference between the observed and calculated fields is now ± 0.8 mGal as a result of incorporation of 2.95 g/cm^3 blocks below Moho into the model. This way of difference minimization is preferred to modeling of crust density variations because the serpentinization of upper mantle is considered as the main process explaining wider flat spot anomalies above the basement highs, exceeding its typical amplitude irregularities and associated to lower Bouguer anomalies values (Fig. 7a). Also, the presence of sedimentary cover ver-

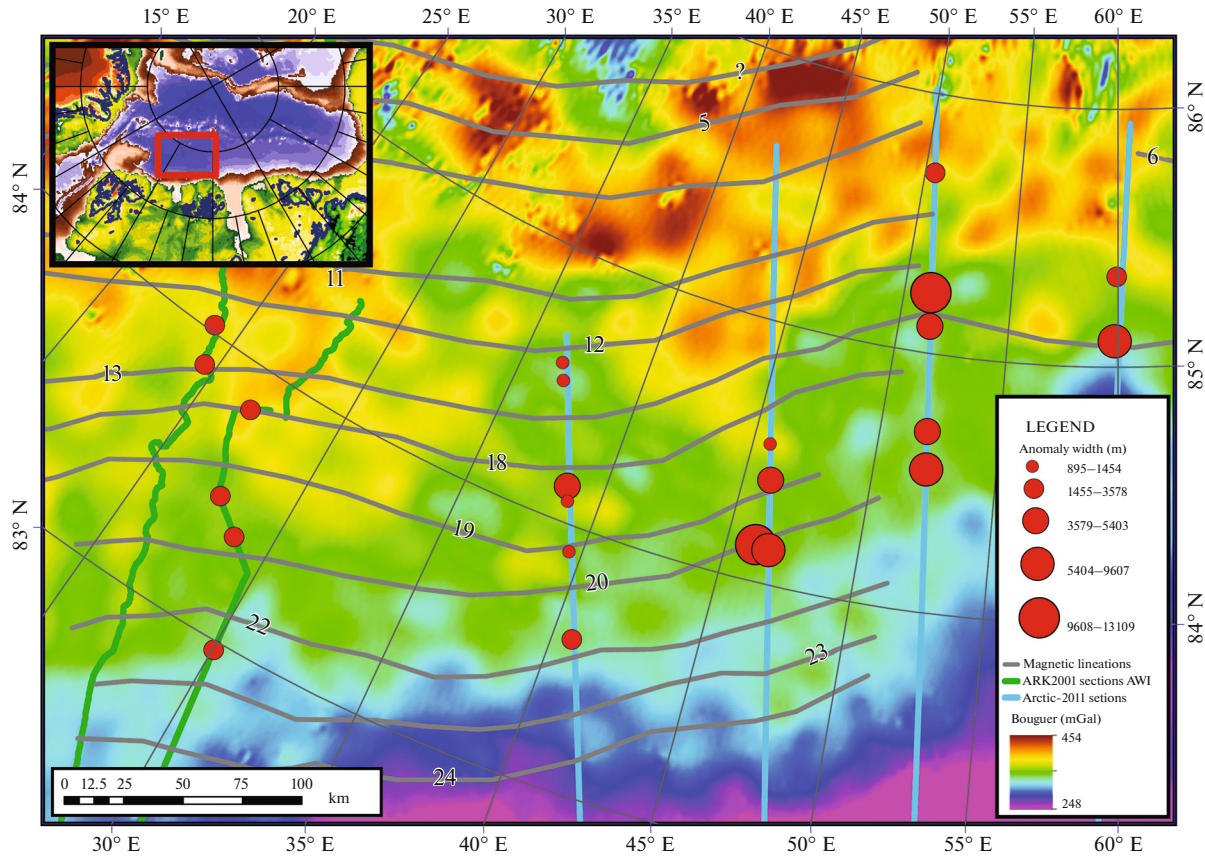


Fig. 9. Spatial distribution of flat spot anomalies with linear scaling of symbols by parameter 3 (spot width). Position of linear magnetic anomalies is after (Jokat and Micksch, 2004). The Bouguer anomalies are after (Balmino et al., 2012). The conditional minimum and maximum sizes of symbols do not coincide with the real sizes of parameters in a map scale.

tical displacements (Fig. 4) supports the assumption of serpentinized blocks volume expansion.

The comparison of modeling results along the Arktika-2011-03 line (Fig. 10) with position of flat spots in sedimentary cover shows that they are mostly focused above the highs of the acoustic basement, the direct gravity effect from which was calculated assuming the upper mantle blocks with a density of 2.95 g/cm^3 . These comparative results of the anomalies with calculated gravity field are consistent with suggestions on their genesis as a result of serpentinization, even without support from drilling of the fluid-saturated sequence.

6. DISCUSSION AND GEODYNAMIC INTERPRETATION

Multichannel seismic data combined with 2D gravity modeling and magnetic isochrone data allowed the model of the structure and evolution of the basement of the Nansen Basin with a significant role of an upper mantle serpentinized layer with a density of 2.95 g/cm^3 . Fluids or gas can also migrate from deep sedimentary layers in the local troughs towards the basement highs.

Deep sedimentary units could contain organic carbon to be a source rock, but in this case the typical hydrocarbon generation conditions of pressure and temperature should be considered to explain appearance of the gas, which is questionable for the region. Currently appearance of conventional hydrocarbon accumulations in standard oceanic crust areas at distance $>150 \text{ km}$ from shelf edges is almost not known.

The flat spot anomalies of seismic sections, which have fluid origin and occur below the seafloor at the depth of gas hydrate stability zone, can be explained as a result of serpentinization of the upper mantle rocks. Unlikely that rough top of lithological inhomogeneous debris flow deposits could serve as horizontal boundary for fluid trap and flat spot anomaly: it could be a physical boundary of gas hydrate stability zone, which can be hosted in part of section with no clear bed boundaries and across them. Process of serpentinization is accompanied by generation of fluids, density loss and vertical displacement of crustal blocks, visible in reflection phases shifts, and formation of faults in sedimentary cover. The presence of these mantle zones is confirmed by 2D gravity modeling (Fig. 10b), the results of which coincide with spa-

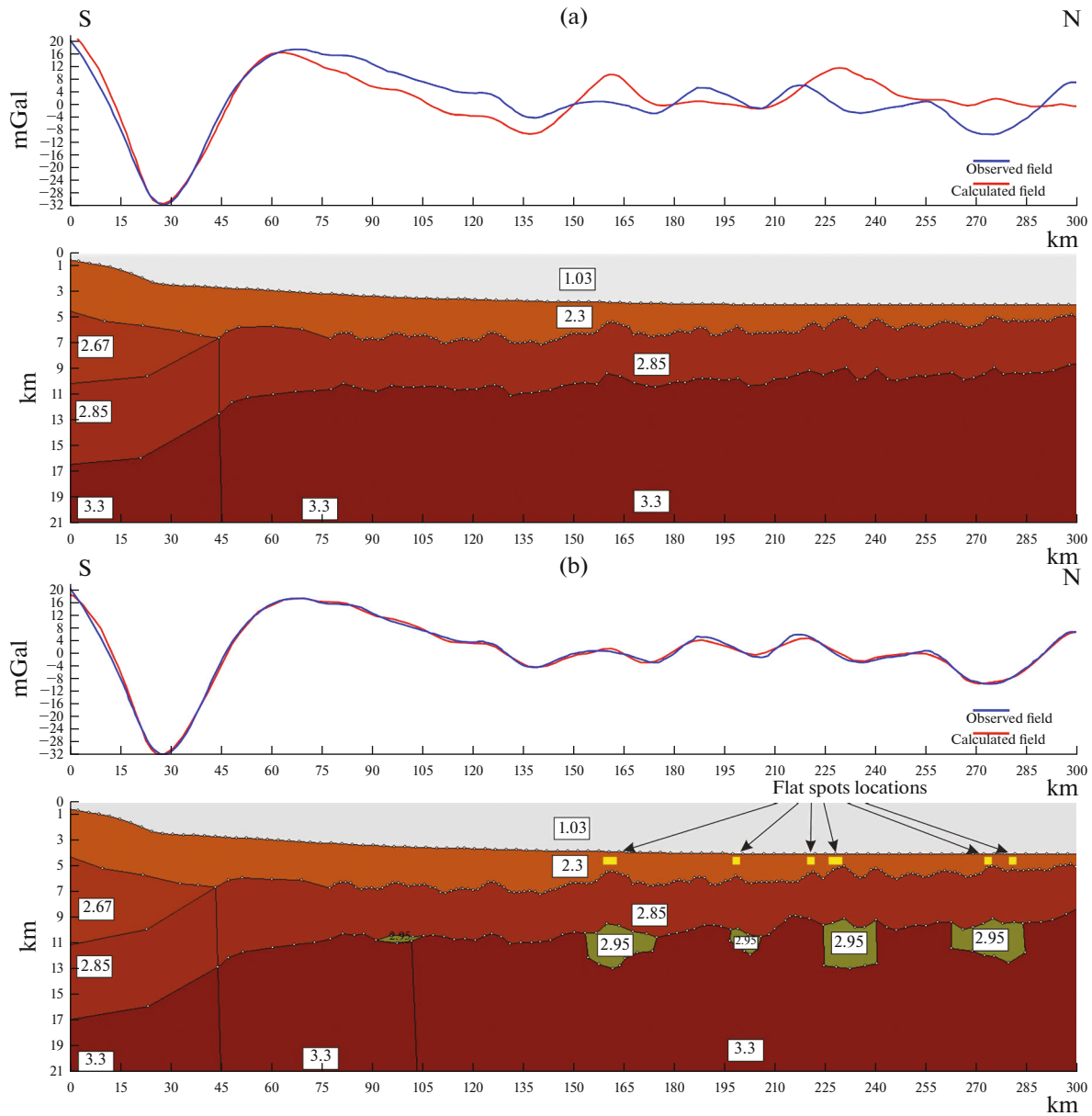


Fig. 10. Results of 2D gravity modeling along the Arktika 2011-03 seismic section: (a) plots of observed free air (Balmino et al., 2012) and calculated anomalies from 4-layer density model: water, sedimentary cover from bottom to acoustic basement detected from seismic data, 4000 m constant thickness crust layer and upper mantle; (b) same layers configuration with added density reduced upper mantle blocks providing optimal coincidence between modeled and observed field and position of flat spots according to seismic data.

tial distribution of flat spots along the section. These data in the studied area could indicate the modern intraplate tectonic activity that makes available faulting and water access to upper mantle. According to (Rajan et al., 2012), similar results come from the formation of mantle detachments in the eastern flank of the Knipovich Ridge. These detachments could be explained by reconfiguration of rift axis with shear components of adjacent tectonic plates movements (Sokolov et al., 2017). According to (Kandilarov et al., 2010) low seismic velocities of the upper mantle are

observed with serpentinization zones, local basement uplifts and seismic record anomalies typical for the presence of fluids in sedimentary cover with total thickness of up to 2.5 s of two-way traveltime. It is noteworthy that the detachments are exposed on the surface of the crystalline crust in the basement area with slowest spreading (half rates of ~5 mm/year) (Kandilarov et al., 2008). The average distance between anomalies C12 and C20 in the Nansen Basin is ~100 km (Fig. 6) meaning that the average spreading half rates was ~10 mm/year over a period from 43 to

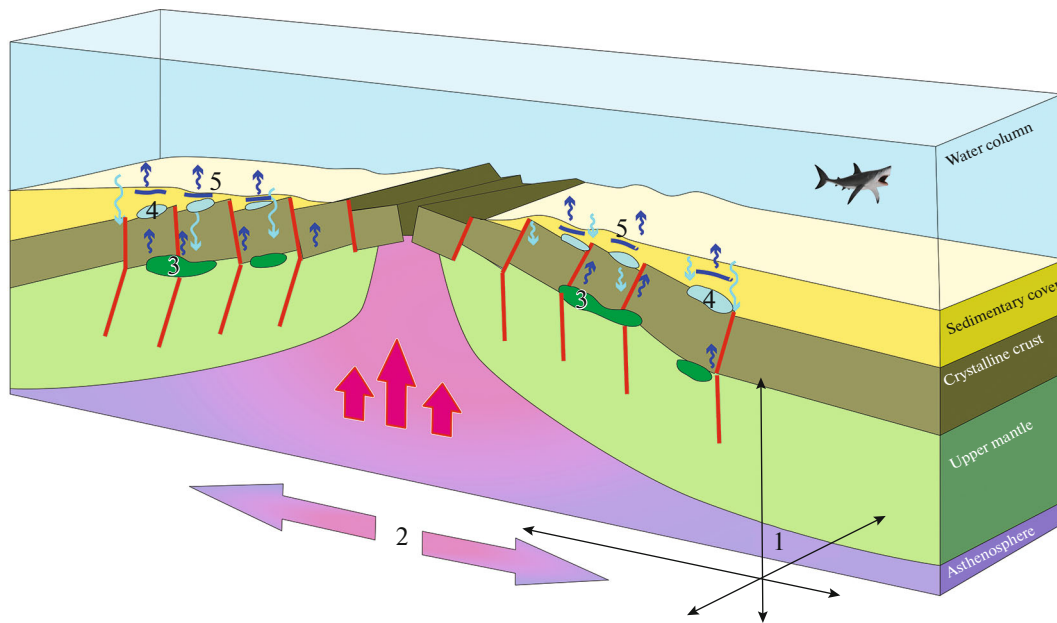


Fig. 11. Consistent causal link of processes occurring inside the layered and blocky lithosphere: (1) contrasting horizontal and vertical rheology of mantle; (2) plate dynamics with horizontal and vertical movements; (3) penetration of water along the faults, serpentinization density reduction of upper mantle; (4) vertical uplift of basement blocks, deformations of sedimentary cover and generation of fluids; (5) subsurface accumulation of fluids, formation of seismic anomalies and fluid penetration into water column.

33 Ma. The distribution of the indexed anomalies within this period, however, is uneven indicating possible significant deviations from the average rates in the basin.

According to *P*-wave seismic tomography data (Jakovlev et al., 2012) Arctic region, Gakkel Ridge and Nansen Basin are the areas with heterogeneous mantle structure. A depth range from 200 to 400 km exhibits the negative velocity anomalies, which occurs in our area of study. Further to the east from the longitude of $\sim 70^\circ$ E, the negative anomalies at these depths are replaced by positive ones, therefore, forming a transition in rheological mantle condition in contrast to the lower depths (< 200 km). It is likely that this contrasting condition below the Cenozoic lithosphere of the Nansen basin also exists in the crust because of the eastward amagmatic transition along the Gakkel Ridge at longitudes of $\sim 40^\circ$ to $\sim 65^\circ$ E according to geochemistry of basalts (Michael et al., 2003). In area of $\sim 85^\circ$ E, this contrasting condition is expressed in a broad field of igneous rocks, the eruption of which was accompanied by earthquakes cluster of 1999 (Schlindwein, 2012). These data confirm highly heterogeneous mantle rheology beneath the elastic lithosphere in the study area from $\sim 40^\circ$ to $\sim 60^\circ$ E (Fig. 1) which could impact on intraplate tectonic processes while moving of lithospheric plates above it.

According to various geophysical data, the intraplate tectonic displacements of basement blocks make a consistent causal link of processes occurring

inside the layered and blocky lithosphere (Fig. 11) and, finally, leading to the formation of flat spots: (1) contrasting horizontal and vertical rheological mantle condition; (2) variable in time and heterogeneous plate dynamics with horizontal and vertical movements of individual blocks of cooled lithosphere and enhanced macro-fracturing in form of detachments; (3) penetration of water along the faults, serpentinization of upper mantle rocks, and origination of density reduction zones; (4) deformations of sedimentary cover generated by vertical uplift of basement blocks and generation of fluids; (5) accumulation of fluids in subsurface sedimentary cover, sparsely injecting into water column, and formation of anomalies of seismic acoustic flat spot record (Sokolov, 2017, 2018).

Flat spots were identified in the area with a narrow basement age range of 43–33 Ma. The age of 33 Ma corresponds to the start of Greenland separation from the Svalbard Plate (Engen et al., 2008). Similar anomalies are not observed above the younger basement within the studied Nansen Basin. It shows that the structure of oceanic basement prior to the opening processes occurred in favorable conditions for the formation of serpentinized blocks in the upper mantle, which leads to the formation of gas-rich environment and is reflected as flat spots in seismic record. It could point to changes of tectonic regime parameters after the breakup and initiation of Arctic basin open status.

7. CONCLUSIONS

1. The flat spot seismic anomalies observed in the Nansen Basin are of fluid origin according to the following seismic indications: negative polarity of the seismic signal, distinct from seafloor reflections, smooth horizontal orientation of the anomalies and location of the anomalies within the sedimentary unit unrelated to lithological reflectors. It can be interpreted as the bottom of gas hydrate stability zone trapping free gas. The depth of the top of the anomalies below the seafloor has almost constant value of 490 ± 100 ms (~ 390 m) and is located in the middle part of seismic unit NB-4. This indicates the ascent of gases from the basement to a common subsurface fluid barrier from various depths of the acoustic basement. The depth of the anomalies below the seafloor corresponds to the theoretical thickness of gas hydrate stability zone in the studied region. The lateral extent of gas reservoirs increases eastward.

2. Flat spot anomalies occur exclusively in a band between spreading anomalies C20 and C12. No anomalies occur in the upper part of sedimentary cover outside of this band above elder basement, where the thickness exceeds 3 km, as well as above the basement younger than C12.

3. Serpentinization of the upper mantle ultramafic rocks is a geochemical process, which can explain the generation and accumulation of methane, observed in the seismic data used for this study, as well as vertical movements of the basement blocks due to density reduction and expansion of the serpentinized rock.

4. The comparison of flat spots morphometric characteristics and Bouguer anomalies show, that evolution of serpentinization processes, identified from it, resulted in increasing gas accumulation in wider flat spots and decrease of the amplitudes of basement highs, probably, due to expanded area around the primary serpentinization center with local density reduction of upper mantle, increasing of total sediment thickness below the wide flat spots and their allocation on mainly positive magnetic anomalies of basement.

5. Gravity modeling results coincide with the observed field, if the crystalline crustal layer has a constant thickness of 4000 m and a density of 2.85 g/cm^3 and the upper mantle blocks with a lower (to 2.95 g/cm^3) density occur below the acoustic basement highs in the upper mantle with a normal density of 3.3 g/cm^3 .

ACKNOWLEDGMENTS

We are grateful to anonymous reviewers for their remarks that helped to improve a previous version of the manuscript. We thank A.A. Bulychev and A.N. Zaitsev for possibility of 2D gravity modeling in TG-2D software (Moscow State University, Department of Geophysical Methods of Earth Crust Study). This work was completed in collaboration of the Geological Institute, Russian Academy of Sciences, and Alfred Wegener Institute Helmholtz

Centre for Polar and Marine Research. The authors would like to thank Emerson E&P Software, Emerson Automation Solutions providing licenses in the scope of the Emerson Academic Program. We also are grateful to Dobrolyubova K.O. for the state-of-art performance of concept figure. We would like to thank Russian Federal Geological Foundation (RFGF) (<https://rfgf.ru>) for access to seismic surveys at Arctic Ocean for implementation of research. The data that support this study are available from this data holder upon reasonable request.

FUNDING

This work was supported by the Russian Foundation for Basic Research (RFBR project no. 18-05-70040) and Russian State Research Programm (project no. FMUN-2019-0076).

REFERENCES

- Arkticheskii bassein (geologiya i morfologiya)* (The Arctic Basin: Geology and Morphology), Kaminskii, V.D, Piskarev, A.L, and Poselov, V.A, Eds., St. Petersburg.: VNIIOkeanologiya. 2017.
- Astafurova, E.G., Gorodnitskii, A.M., Luk'yanov, S.V., and Mashchenkov, S.P., Nature of magnetic anomalies in the oceanic crust of the Mid-Atlantic Ridge and adjacent depressions within the Canary-Bahamas geotraverse, in *Priroda magnitnykh anomalii i stroenie okeanicheskoi kory* (Nature of Magnetic Aand Structure of the Oceanic Crust), Gorodnitskii, A.M., Ed., VNIRO, 1996, pp. 171–202.
- Astafurova, E.G., Gurevich, N.I., Daniel, E.D., and Mashchenkov, S.P., Cmparison of features of the oceanic crust accretion during the ultra-slow spreading, *Ross. Zh. Nauk Zemle*. 2000, vol. 2, no.3, pp. 295–301.
- Backus, M.M. and Chen, R.L., Flat spot exploration, *Geophys. Prosp.*, 1975, vol. 23, no. Iss. 3, pp. 533–577.
- Balmino, G., Vales, N., Bonvalot, S., and Briais, A., Spherical harmonic modeling to ultra-high degree of Bouguer and isostatic anomalies, *J. Geod.*, 2012, vol. 86, pp. 499–520.
- Baranov B.V., Lobkovskii L.I., Dozorova D.A., Tsukanov N.V. The Fault System Controlling Methane Seeps on the Shelf of the Laptev Sea, *Dokl. Earth Sci.* 2019, vol. 486, no. 3, pp. 571–574.
<https://doi.org/10.31857/0869-56524863354-358>
- Baturin, D., Fedukhina, T., Savostin, L., and Yunov, A., A geophysical survey of the Spitsbergen margin and surrounding areas, *Mar. Geophys. Res.*, 1994, vol. 16, pp. 463–484.
- Bougault, H., Hydrogène et methane hydrothermal: Enjeux scientifiques une ressource potentielle nouvelle?, *Mines Carr. Industr. Miner.*, 2012, no. 196, pp. 73–80.
- Bulychev A.A., Zaitsev A.N. Program for the intwervative 2D selection of density medium vased on the anomalous gravity field, in *Svidetel'stvo o gosudarstvennoi registratsii programmy dlya EVM no. 2008611947* (State Registration Program for Computers. Certificate No. 2008611947), April, 2008.
- Burguto, A. G., Zhuravlev, V. A., Zavarzina, G. A., Zinchenko, A. G., et al., *Gosudarstvennaya geologicheskaya karta Rossiiskoi Federatsii. Masshtab 1 : 1000000* (State geo-

- logical Map of the Russian Federation. Scale 1 : 1000000), St. Petersburg: VSEGEI, 2016, Ser. North Kara–Barents Sea. Sheet S-36, S-37—Barents Sea. Explanatory Note.
- Castro, C.F., Knutz, P.C., Hopper, J.R., and Funck, T., Depositional evolution of the western Amundsen Basin, Arctic Ocean: Paleooceanographic and tectonic implications, *Paleoceanogr. Paleoclimatol.*, 2018, vol. 33, no. 12, pp. 1357–1382.
- Charlou, J.L., Fouquet, Y., Bougault, H., et al., Intense CH₄ plumes generated by serpentinization of ultramafic rocks at the intersection of the 15°20' N fracture zone and the Mid-Atlantic Ridge, *Geochim. Cosmochim. Acta*, 1998, vol. 62, no. 13, pp. 2323–2333.
- Cherkashev, G.A., Gusev, E.A., Zhirnov, E.A., et al., The Knipovich Ridge rift zone: Evidence from the Knipovich-2000 expedition, *Dokl. Earth Sci.*, 2001, vol. 378, pp. 420–423.
- Curewitz, D., Okino, K., Asada, M., et al., Structural analysis of fault populations along the oblique, ultra-slow spreading Knipovich Ridge, North Atlantic Ocean, 74°30' N–77°50' N, *J. Struct. Geol.*, 2010, vol. 32, pp. 727–740.
- Czuba, W., 2.5-D seismic tomographic modelling of the crustal structure of north-western Spitsbergen based on deep seismic soundings, *Mar. Geophys. Res.*, 2007, vol. 28, pp. 213–233.
- Delescluse, M. and Chamot-Rooke, N., Serpentinization pulse in the actively deforming Central Indian Basin, *Earth Planet. Sci. Lett.*, 2008, vol. 276, pp. 140–151.
- Dick, H., Lin, J., and Schouten, H., An ultraslow-spreading class of ocean ridge, *Nature*, 2003, vol. 426, pp. 407–412.
- Dmitriev, L.V., Bazylev, B.A., Silant'ev, S.A., et al., The formation of hydrogen and methane during the serpentinization of mantle hyperbasites in the ocean and origin of oil, *Ross. Zh. Nauk Zemle*, 1999, vol. 1, no. 6, pp. 511–519. <https://doi.org/10.2205/2000ES000030>
- Edwards, M.H., Kurras, G.J., Tolstoy, M., et al., Evidence of recent volcanic activity on the ultra-slow spreading Gakkkel Ridge, *Nature*, 2001, vol. 409, pp. 808–812.
- Engen, Ø., Faleide, J.I., and Dyreng, T.K., Opening of the Fram Strait gateway: A review of plate tectonic constraints, *Tectonophysics*, 2008, vol. 450, pp. 51–69.
- Engen, Ø., Gjengedal, J.A., Faleide, J.I., et al., Seismic stratigraphy and sediment thickness of the Nansen Basin, Arctic Ocean, *Geophys. J. Int.*, 2009, vol. 176, pp. 805–821.
- Faust, L.Y., Seismic velocity as a function of depth and geologic time, *Geophysics*, 1951, vol. 16, no. 2, pp. 192–206.
- Fizicheskie svoystva gornykh porod i poleznykh iskopaemykh (petrofizika). Spravochnik geofizika (Physical Properties of Rocks and Mineral Resources (Petrophysics): Handbook. Geophysics)*, Dortman, N.B., Ed., Moscow: Nedra, 1984.
- Gardner, G.H.F., Gardner, L.W., and Gregory, A.R., Formation velocity and density—the diagnostic basics for stratigraphic traps, *Geophysics*, 1974, vol. 39, no. 6, pp. 770–780.
- Geissler, W.H. and Jokat, W., A geophysical study of the northern Svalbard continental margin, *Geophys. J. Int.*, 2004, vol. 158, pp. 50–66.
- Hegewald, A. and Jokat, W., Relative sea level variations in the Cukchi region—Arctic Ocean—since the late Eocene, *Geophys. Rev. Lett.*, 2013, vol. 40, pp. 803–807. <https://doi.org/10.1002/GRL.50182>
- Hermann, T. and Jokat, W., Crustal structures of the Boreas Basin and the Knipovich Ridge, North Atlantic, *Geophys. J. Int.*, 2013, vol. 193, pp. 1399–1414.
- Jackson, H.R., Johnson, G.L., Sundvor, E., and Myhre, A.M., The Yermak Plateau—formed at a triple junction, *J. Geophys. Res.*, 1984, vol. 89, pp. 3223–3232.
- Jakobsson, M., Mayer, L., Coakley, B., et al., The International Bathymetric Chart of the Arctic Ocean (IBCAO) Version 3.0, *Geophys. Rev. Lett.*, 2012, vol. 39, no. 12, pp. 1–6.
- Johnson, J.E., Mienert, J., Plaza-Faverola, A., et al., Abiotic methane from ultraslow-spreading ridges can charge Arctic gas hydrates, *Geology*, 2015, vol. 43, no. 5, pp. 371–374.
- Jokat, W. and Micksch, U., Sedimentary structure of the Nansen and aAmundsen basins, Arctic Ocean, *Geophys. Rev. Lett.*, 2004, vol. 31, p. L02603.
- Jokat, W., Weigelt, E., Kristoffersen, Y., et al., New geophysical results from the south-western Eurasian Basin (Morris Jesup Rise, Gakkkel Ridge, Yermak Plateau) and the Fram Strait, *Geophys. J. Int.*, 1995, vol. 123, pp. 601–610.
- Jokat, W., Ritzmann, O., Schmidt-Aursch, M.C., et al., Geophysical evidence for reduced melt production on the Arctic ultraslow Gakkkel Mid-Ocean Ridge, *Nature*, 2003, vol. 423, pp. 962–965.
- Judd, A.G. and Hovland, M., *Seabed Fluid Flow: The Impact on Geology, Biology, and the Marine Environment*, Cambridge: Cambr. Univ. Press, 2007.
- Kandilarov, A., Mjelde, R., Okino, K., and Murai, Y., Crustal structure of the ultra-slow spreading Knipovich Ridge, North Atlantic, along a presumed amagmatic portion of oceanic crustal formation, *Mar. Geophys. Res.*, 2008, vol. 29, pp. 109–134.
- Kandilarov, A., Landa, H., Mjelde, R., et al., Crustal structure of the ultra-slow spreading Knipovich Ridge, North Atlantic, along a presumed ridge segment center, *Mar. Geophys. Res.*, 2010, vol. 31, pp. 173–195.
- Karta dochetvertichnykh obrazovaniy, vol-37-40 (Zemlya Frantsa-Iosifa, yuzhnye ostrova). Gosudarstvennaya geologicheskaya karta Rossiiskoi Federatsii masshtaba 1 : 1000000 (novaya seriya). List 1 (Map of Pre-Quaternary Deposits. T-37–40 (Franz Josef Land, Southern Islands). State Geological Map of the Russian Federation. Scale 1 : 1000000 (New Series). Sheet 1), Lopatin, B.G., Ed., St. Petersburg: VNII-Morgeo, 2004.*
- Keir, R.S., Greinert, J., Rhein, M., et al., Methane and methane carbon isotope ratios in the Northeast Atlantic including the Mid-Atlantic Ridge (50° N), *Deep-Sea Res. I*, 2005, vol. 52, pp. 1043–1070. <https://doi.org/10.1016/j.dsr.2004.12.006>
- Khutorskoi, M.D., Akhmedzyano, V.R., Ermakov, A.V., et al., *Geotermiya arkticheskikh morei (Geotectonics of Arctic Seas)*, Moscow: GEOS, 2013.
- Klein, E.M., Earth science: Spread thin in the Arctic, news and views, *Nature*, 2003, vol. 423, pp. 932–933.
- Kuo, B.Y. and Forsyth, D.W., Gravity anomalies of the ridge-transform system in the South Atlantic between 31° and 34.5° S: Upwelling centers and variations in crustal thickness, *Mar. Geophys. Res.*, 1988, vol. 10, pp. 205–232.
- Ljones, F., Kuwano, A., Mjelde, R., Breivik, A., and Shimamura, H., Crustal transect from the North Atlantic Kni-

- povich Ridge to the Svalbard margin west of Hornsund, *Tectonophysics*, 2004, vol. 378, pp. 17–41.
- Lutz, R., Franke, D., Berglar, K., Heyde, I., Schreckenberger, B., Klitzke, P., and Geissler, W.H., Evidence for mantle exhumation since the early evolution of the slow-spreading Gakkel Ridge, Arctic Ocean, *J. Geodyn.*, 2018, vol. 118, pp. 154–165.
- Maus, S., Barckhausen, U., Berkenbosch, H., et al., EMAG2: A 2-arc-minute resolution Earth Magnetic Anomaly Grid compiled from satellite, airborne and marine magnetic measurements, *Geochem. Geoph. Geosyst. G3*, 2009, vol. 10, no. 8, pp. 1–12.
- Michael, P.J. and Langmuir, C.H.B., Dick, H.J., et al., Magmatic and amagmatic seafloor generation at the ultraslow-spreading Gakkel Ridge, Arctic Ocean, *Nature*, 2003, vol. 423, pp. 956–961.
- Moore, T.E. and Pitman, J.K., Geology and petroleum potential of the Eurasia Basin, *Geol. Soc. Mem.*, 2011, vol. 35, pp. 731–750.
- Myhre, A.M., Thiede, J., Firth, J.V., et al., Site 911, *Proc. Ocean Drill. Progr., Init. Rep.*, 1995, vol. 151, pp. 271–318.
- Nikishin, A.M., Malyshev, N.A., and Petrov, E.I., Main issues in the structure and history of the geological evolution of the Arctic Ocean, *Vestn. Ross. Akad. Nauk.* 2020, vol. 90, no. 5, pp. 434–446.
<https://doi.org/10.1134/S101933162003003X>
- Nikishin, A.M., Gaina, C., Petrov, E.I., et al., Eurasia Basin and Gakkel Ridge, Arctic Ocean: Crustal asymmetry, ultra-slow spreading and continental rifting revealed by new seismic data, *Tectonophysics*, 2017, vol. 746, no. 10, pp. 64–82.
- Okino, K., Curewitz, D., Asada, M., et al., Preliminary analysis of the Knipovich Ridge segmentation: influence of focused magmatism and ridge obliquity on an ultraslow spreading system, *Earth Planet. Sci. Lett.*, 2002, vol. 202, pp. 275–288.
- Oufi, O., Cannat, M., and Horen, H., Magnetic properties of variably serpentinized abyssal peridotites, *J. Geophys. Res.*, 2005, vol. 107, no. B5.
- Petrov, O., Morozov, A., Shokalsky, S., Kashubin, S., Artemieva, I., Sobolev, N., Petrov, E., Ernst, R., Sergeev, S., and Smelror, M., Crustal structure and tectonic model of the Arctic region, *Earth-Sci. Rev.*, 2016, vol. 154, pp. 29–71.
- Rajan, A., Mienert, J., Bunz, S., and Chand, S., Potential serpentinization, degassing, and gas hydrate formation at a young (<20 Ma) sedimented ocean crust of the Arctic Ocean ridge system, *J. Geophys. Res.*, 2012, vol. 117, p. B03102.
<https://doi.org/10.1029/2011JB008537>
- Riis, F., North of Nordaustlandet, in *Seismic Atlas of Western Svalbard: A Selection of Seismic Transects, Meddelelser*, Eiken, O., Ed., *Norsk Polarinst.*, 1994, vol. 130, pp. 30–31.
- Ritzmann, O., Jokat, W., Mjelde, R., and Shimamura, H., Crustal structure between the Knipovich Ridge and the Van Mijenfjorden (Svalbard), *Mar. Geophys. Res.*, 2002, vol. 23, pp. 379–401.
- Ritzmann, O., Jokat, W., Czuba, W., et al., A deep seismic transect from Hovgard Ridge to northwestern Svalbard across the continental-ocean transition: A sheared margin study, *Geophys. J. Int.*, 2004, vol. 157, pp. 683–702.
- Schindwein, V., Teleseismic earthquake swarms at ultraslow spreading ridges: indicator for dyke intrusions?, *Geophys. J. Int.*, 2012, vol. 190, pp. 442–456.
- Schmidt-Aursch, M. and Jokat, W., 3D gravity modelling reveals off-axis crustal thickness variations along the western Gakkel Ridge (Arctic Ocean), *Tectonophysics*, 2016, vol. 691, pp. 85–97.
- Shakhova, N., Semiletov, I.P., Gustafsson, O., et al., Current rates and mechanisms of subsea permafrost degradation in the East Siberian Arctic shelf, *Nat. Commun.*, 2017, p. 8.
- Snow, J.E. and Edmonds, H.N., Ultraslow-spreading ridges: rapid paradigm changes, *Oceanography*, 2007, vol. 20, no. 1, pp. 90–101.
- Sokolov, S.Yu., Tectonic zoning of Wrangel Island, Arctic region, *Geotectonics*, 2017, no. 1, pp. 3–16.
- Sokolov, S.Yu., *Tektonika i geodinamika Ekvatorial'nogo segmenta Atlantiki* (Tectonics and Geodynamics of the Atlantic Equatorial Segment), Moscow: Nauchn. Mir, 2018.
- Sokolov, S.Yu., Sedimentary cover deformations in the Equatorial Atlantic and their comparison with geophysical fields, *Geotectonics*, 2017, vol. 51, no. 1, pp. 74–88.
- Sokolov, S.Yu., Abramova, A.S., Moroz, E.A., and Zarskaya, Yu.A., Amplitudes of faulting on walls of the Knipovich Ridge (North Atlantic): An indicator of recent regional dynamics, *Geodinam. Tektonofiz.*, 2017, vol. 8, no. 4, pp. 769–789.
- Sokolov, S.Yu., Geissler, V.Kh., and Abramova, A.S., Flat spots in the Nansen Basin associated with ultra-slow spreading and serpentinization, *Proc. XXIII Int. Sci. School Marine Geology*, Moscow: IO RAN, 2019, vol. 2, pp. 190–194.
- Sorokin, M.Y., Zamansky, Y.Y., Languinen, A.Y., et al., North Pole–28 ice drift seismic line, *Abstracts of Papers, ICAM III Third Int. Conf. Arctic Margins*, Celle, pp. 12–16.
- Startseva, K.F., Nikishin, A.M., Malyshev, N.A., et al., Geological and geodynamic reconstruction of the East Barents Megabasin from analysis of the 4-AR regional seismic profile, *Geotectonics*. 2017, no. 4, pp. 383–397.
- Taner, M.T., Koehler, F., and Sheriff, R.E., Complex seismic trace analysis, *Geophysics.*, 1979, vol. 44, no. 6, pp. 1041–1063.
- Waghorn, K.A., Bunz, S., Plaza-Faverola, A., and Johnson, J.E., 3D seismic investigation of a gas hydrate and fluid flow system on an active mid-ocean ridge: Svyatogor Ridge, Fram Strait, *Geochem., Geoph., Geosyst.*, 2018, vol. 19, no. 8, pp. 2325–2341.
- Wallmann, K., Pinero, E., Burwicz, E., et al., The global inventory of methane hydrate in marine sediments: a theoretical approach, *Energies*, 2012, vol. 5, pp. 2449–2498.
- Weigelt, E. and Jokat, W., Peculiarities of roughness and thickness of oceanic crust in the Eurasian Basin, Arctic Ocean, *Geophys. J. Int.*, 2001, vol. 145, pp. 505–516.
- Yakovlev, A.V., Bushenkova, N.A., Kulakov, I.Yu., and Dobretsov, N.L., Structure of the upper mantle in the Arctic region: Based on regional seismotomography, *Geol. Geofiz.*, 2012, vol. 53, no. 10, pp. 1261–1272.